Turbulence Properties of the Impeller Stream of a Rushton Turbine

K. C. Lee and M. Yianneskis
Department of Mechanical Engineering, King's College London, London WC2R 2LS, U.K.

The structure of the flow in a vessel stirred by a Rushton turbine was investigated using laser Doppler anemometry measurement techniques. The time and length scales of turbulence were determined and used to estimate the dissipation rate of turbulence energy. The levels of turbulence energy and dissipation are high near the turbine and decrease rapidly with increasing distance from the turbine blades. The turbulence in the impeller stream is mostly anisotropic close to the blades. The results are compared with the findings of earlier investigations, and their implications for computational fluid dynamics (CFD) predictions of the flows are discussed.

Introduction

The complex nature of the flowfields in stirred chemical reactors has motivated a number of studies of the mean velocity and turbulence characteristics of the flows produced by different impeller designs. In particular, a large body of knowledge has been accumulated on the flow in vessels stirred by a single Rushton impeller, as this impeller design has been used for a wide range of industrial processes (see, for example, Cutter, 1966; van't Riet and Smith, 1975; van't Riet et al., 1976; Yianneskis et al., 1987; Mahouast et al., 1989; Wu and Patterson, 1989; Yianneskis and Whitelaw, 1993; Stoots and Calabrese, 1995; Rutherford et al., 1996b).

These investigations have identified the formation of a trailing vortex pair behind each impeller blade and that the ensemble-averaged turbulence levels measured in the impeller stream may be overestimated by the associated variation in mean velocity (pseudo-turbulence). Even though the flow in the impeller vicinity of stirred reactor vessels is periodic, ensemble-averaged LDA (laser Doppler anemometry) measurements obtained over 360° of impeller revolution are widely employed for the description of the velocity and turbulence fields. These measurements do not account for the pseudo-turbulence due to the passage of the impeller blades (Van't Riet et al., 1976; Yianneskis et al., 1987; Stoots and Calabrese, 1995; Yianneskis and Whitelaw, 1993) which performed angle-resolved LDA measurements over 60° of impeller revolution where the data were arranged in 1° averages. Such angle-resolved measurements do show the variation of the mean flow velocities and the turbulence fluctuations with blade angle ϕ. It has been shown that in comparison with 1° angle-resolved measurements, 360° ensemble-averaged measurements can lead to an overestimation of turbulence quantities in the impeller stream by up to 400% (Yianneskis and Whitelaw, 1993). In addition, time-resolved data can be used to obtain information about the frequency content of the velocity fluctuations and to calculate turbulence quantities of interest. Therefore, in this investigation measurements were primarily obtained as angle-resolved (that is, ensemble-averages over intervals of 1° of revolution) mean velocities and turbulence levels, and as time-resolved velocity recordings.

Most of the investigations reported to date have been concerned with the mean flow structure and the normal turbulence stresses only. Quantities important for micromixing such as the length- and time-scales of turbulence and the dissipation rate of the turbulence kinetic energy have received less attention, partly due to the difficulties associated with their measurement. Mahouast et al. (1989), Wu and Patterson (1989), and Stoots and Calabrese (1996), for example, have measured turbulent shear stresses and/or estimated length scales and dissipation rates, but the understanding of the turbulence structure is still far from complete.

The objective of the present study is to characterize the nature of the turbulence in the discharge stream of a Rushton impeller by compiling a comprehensive set of data of high spatial resolution through angle- and time-resolved LDA measurements to avoid the errors associated with pseudo-turbulence. Comparisons are made with previously reported measurements where appropriate and an attempt is made to

Correspondence concerning this article should be addressed to M. Yianneskis.

quantify the extent of anisotropy of the turbulence in the vessel. The data provide information on quantities which may be used as boundary conditions in and/or for the assessment of CFD predictions of the flows.

Flow Configuration and Experimental Techniques

Stirred vessel configuration

The measurements were made in a cylindrical vessel of diameter $T = 100$ mm, and the liquid height in the vessel was $H = T$ (m). Figure 1a shows the geometry of the mixing vessel, which was identical to the standard configuration used in mixing research (Uhl and Gray, 1966). Four equally spaced vertical baffles of width B (m) $= T/10$ and thickness of 1 mm were fitted along the internal surface of the vessel. The vessel was made of clear cast acrylic plastic (Plexiglass) and was located inside a transparent Plexiglass trough; a flat transparent base was incorporated to maximize optical access. The vessel could be rotated about its axis to enable measurements to be performed at different vertical planes. The gap between the vessel and the trough was filled with distilled water fed from a constant temperature water bath to remove the heat generated by the impellers and thus to maintain the temperature inside the vessel constant during the experiments, as well as to minimize refraction effects at the cylindrical surface of the vessel.

The Rushton turbine was a six-bladed impeller of diameter D (m) $= T/3$, as shown in Figure 1b. Both the blade thickness t_b (m) and the disk thickness t_d (m) were 1 mm. The blade width W(m) was 0.25 D. A clearance C (m) $= T/3$ was used between the bottom of the mixing vessel and the impeller disk plane. The working fluid was distilled water and all measurements were conducted at a Reynolds number of 40,000, which corresponded to a constant impeller rotational speed (rev/min) of $N = 2{,}165 \pm 10$ rpm ($V_{tip} = 3.77$ m/s). The impeller rotated in a clockwize direction as viewed from above.

An optical shaft encoder which provided a marker pulse and a train of 2,000 pulses per revolution was coupled to the impeller shaft. The pulses were input to a specially-built gating unit. By counting the number of marker pulses per unit time, the rotational speed of the impeller could be measured. The midpoint of a blade of the impeller was aligned with the marker pulse, and by counting the number of pulses (1–2,000) relative to the marker pulse, the blade angle ($\phi = 0°$–$60°$) could be determined. The gating unit was also capable of generating a window gate pulse to set the blade angle interval over which measurements were to be obtained.

The origin of the coordinate system used is the center of the base of the vessel. To allow comparisons with measurements made in vessels of different sizes, all distances are normalized with the vessel diameter T, and all locations are described in terms of normalized axial (z/T), normalized radial (r/T) and tangential (θ) coordinates. Measurements of all three velocity components were performed in the $\theta = 0°$ plane, located halfway between two baffles. The angular location of the measurement volume with respect to the leading blade for the angle-resolved measurements is expressed as the angle ϕ: $\phi = 0°$, the vertical plane through the middle of the leading blade.

A transparent lid was located above the liquid surface at a height $H = T$ so that no air bubbles were entrained into the liquid from the free surface. The lack of a free surface enabled measurements to be made in forward scatter when the beam entered through the bottom of the vessel. This was achieved by attaching a mirror above the lid and filling the space above the lid with water so that the mirror was always submerged. The scattered light was redirected by 90° by the mirror. The effect of a lid on the flow in a stirred vessel has

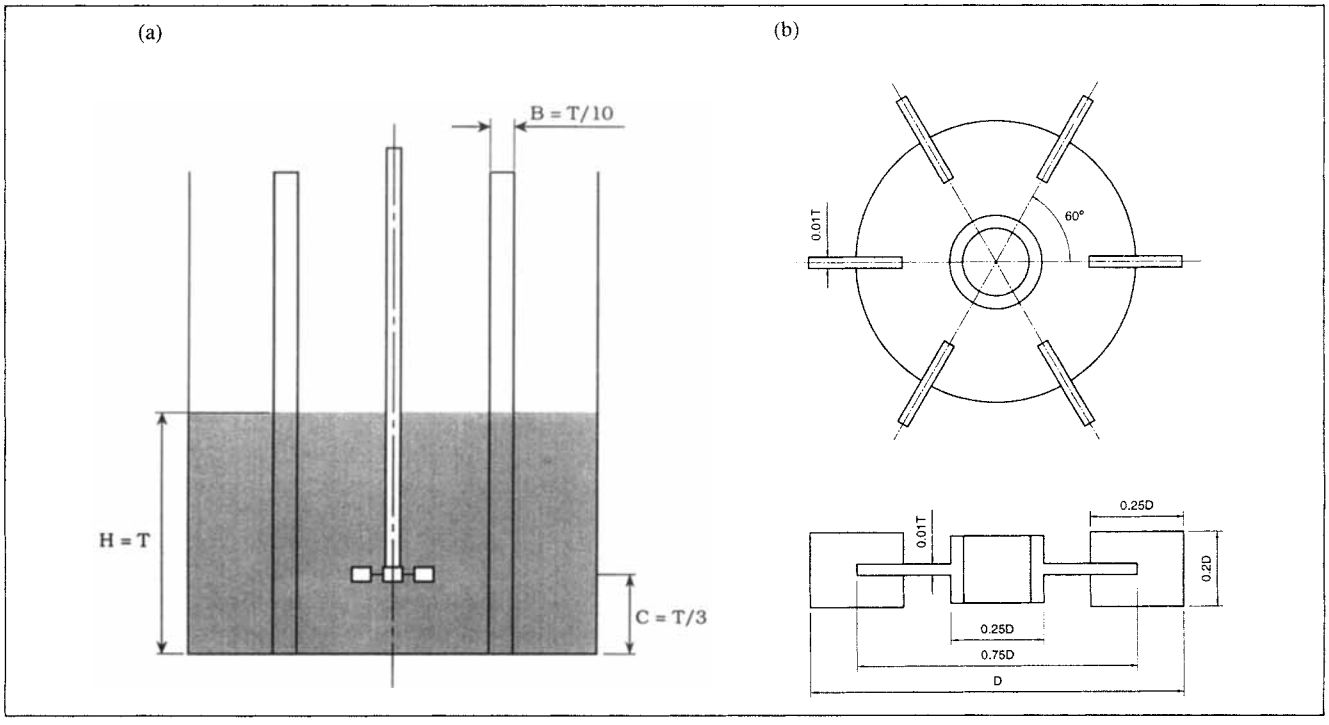

Figure 1. (a) Stirred vessel configuration; (b) impeller geometry.

been previously investigated by Nouri and Whitelaw (1990), who concluded that the use of a lid only affects the flow in the immediate vicinity of the lid/free surface and that the velocities elsewhere in a 144 mm vessel were almost identical to those in a 294 mm vessel.

Angle-resolved measurements were made of the axial, radial and tangential mean velocity (m/s) components ($\overline{U}$, $\overline{V}$, and $\overline{W}$, respectively); and of the corresponding turbulence levels (m/s) (u', v', and w', respectively), at 8,160 locations in the vicinity of the impeller stream. The measuring grid was selected in order to reveal in detail the structure of the trailing vortices while minimizing the measurement time. In order to determine the flow motion relative to the rotating blade, the rotational velocity V_r was subtracted from the angle-resolved mean tangential velocities. V_r was defined as

$$V_r = \frac{2\pi Nr}{60} \text{ (m/s)} \tag{1}$$

where N is the impeller rotational speed in revolutions per minute, and r is the radial distance from the axis of the vessel to the point of measurement.

For the purpose of comparison with data obtained in vessels of different sizes, all angle-resolved mean velocities have been normalized with the blade tip velocity $V_{tip} = \pi ND/60$ (m/s) and are denoted by $\overline{U}/V_{tip}$, $\overline{V}/V_{tip}$, and $\overline{W}/V_{tip}$, respectively, for the axial, radial, and tangential components. The turbulence level results were also normalized with V_{tip} and are denoted by u'/V_{tip}, v'/V_{tip} and w'/V_{tip} for the axial, radial, and tangential components, respectively. Angle-resolved turbulence kinetic energy results were obtained from the u', v', and w' data using

$$k = \frac{1}{2}(u'^2 + v'^2 + w'^2) \tag{2}$$

The turbulence kinetic energy results were normalized with V_{tip}^2 and the corresponding values are denoted by k/V_{tip}^2.

To facilitate interpretation of the results, the outline of a quarter of the impeller disk is drawn to scale in all figures depicting the results obtained in horizontal (z) planes; while in the figures depicting the results obtained in vertical (ϕ) planes, the outline of one-half of the cross-section of the impeller and of the impeller shaft are drawn to scale. In the figures depicting results in z planes, the impeller should be considered to be rotating clockwise, while in those depicting results in ϕ planes, the impeller should be considered to be moving out of the plane of the paper towards the viewer. In order to aid the interpretation of the results, a reference scale having the magnitude of V_{tip} is drawn in each figure depicting angle-resolved mean velocity vectors. Turbulence kinetic energy results are plotted in contour form. To investigate the extent of the periodicity of the flow in the vessel, instantaneous velocity recordings of the radial component V were also made at a number of radii in the $z/T = 0.33$ plane, and their corresponding energy spectra were computed.

Laser Doppler anemometer and experimental techniques

The anemometer comprised a 10-mW Helium-Neon laser, associated lenses, and a radial diffraction grating for splitting and frequency shifting the laser beam. The grating was mounted onto a purpose-built rotating unit, which could be rotated through 135° in steps of 22.5° about the optical axis, thus allowing the plane of the beams to be altered for the measurements of different velocity components. The grating provided a frequency shift of 3.27 MHz between the first-order beams.

The optical bench was mounted on a laboratory jack attached to a compound traversing table and could be traversed in three orthogonal directions. The location of the measurement volume was determined by a well-tested computer program. The displacement of the measurement volume due to refraction, albeit small, varied according to the position of the measurement volume itself and was accounted for at all locations. The accuracy in traversing the optical bench in the two horizontal directions was 0.05 mm and in the z direction 0.1 mm. The bench was aligned to the test section such that the optical axis of the anemometer was contained within a diametrical plane of the vessel (that is, either the $\theta = 0°$ or the $\theta = 180°$ planes), and was perpendicular to a trough wall. The radial and tangential velocity components were measured with the beams entering from the bottom of the vessel with the aid of a mirror situated below the test section at an angle of 45° to the vessel axis, and the axial velocity component was measured with the beams entering from the side of the vessel. In all cases, the beams entered the vessel with their optical axes normal to either the vessel wall or the vessel bottom. By taking into account the refractive index of distilled water (the fluid used as the working fluid and to fill the gap between the vessel and the trough), the position of the measurement volume was determined.

The working fluid was seeded with neutrally buoyant particles (specific gravity = 1.0 ± 0.2) of 3-μm mean diameter. The forward scattered light produced when these particles crossed through the measurement volume was focused by a zoom lens onto a pinhole at the front of the housing of a photomultiplier.

Two types of signal processing were used. A frequency counter (TSI model 1990B) was used for angle-resolved measurements and a Dantec burst spectrum analyzer (BSA) for time-resolved measurements. The signal from the photomultiplier was filtered to remove low frequency pedestal and high frequency noise and then amplified by a variable gain. The quality of the signal was continuously monitored with an oscilloscope. The counter was interfaced with a PC. The interface was controlled by a computer program to acquire data from the counter and the arrival time/angle of the data. The gate window width of the gating unit was set to open to enable acquisition of data between a specified 60° interval (that is, between two neighboring blades).

The number of samples required to achieve statistically independent results depends on the local turbulence intensity, and it was found that at least 500 samples were required for most 1° blade angle intervals. For each measurement, over 60,000 velocity data were collected between the two impeller blades (that is, a 60° angle). The velocity data and their corresponding angles were then saved on a disk file for off-line processing. The uncertainty in aligning the marker pulse with the impeller blade was 0.17°.

The BSA was also interfaced to a PC and could be set up and controlled via software installed in the PC. The software

was also used to acquire data from the BSA, calculate various statistical quantities, and export the acquired data to disk files for off-line processing. The BSA was operated in Burst mode, that is, only one measurement was performed per detected burst, and the measured frequencies were either time stamped or angle stamped. Frequency data was then transformed to velocity data by the software and stored on disk files for off-line processing.

There are a number of possible error sources in an LDA system and measurement uncertainties vary with location and are difficult to calculate precisely. Comparison of measurements obtained with the BSA and with the frequency counter was made in selected locations; the two values were similar (within 2%) in all cases. The variation of impeller speed was kept within ± 10 rpm (0.46%). During any set of measurements, if the variation of speed exceeded these values, the measurements were rejected. The accumulated errors in the mean and rms velocity measurements presented here were estimated to be, on average, 1–3% and 5–10% of V_{tip}, respectively, with the higher errors expected in regions of steep velocity gradients (see also Rutherford et al. (1996a)).

Experimental Results and Discussion

Angle-resolved mean velocity measurements

Although this work is concerned primarily with the turbulence properties of the impeller stream, a brief description of the mean flow field is given below to facilitate interpretation of the results. The mean velocity vectors relative to the blade (that is, with the rotational velocities subtracted from the tangential components) obtained in the $z/T = 0.35$ plane, 2 mm above the impeller disk, are shown in Figure 2. It can be seen that there is a recirculation region behind the leading blade at $r/T = 0.17$ and between $\phi = 0°$ and $\phi = 45°$. This region is associated with the trailing vortex generated behind the blade

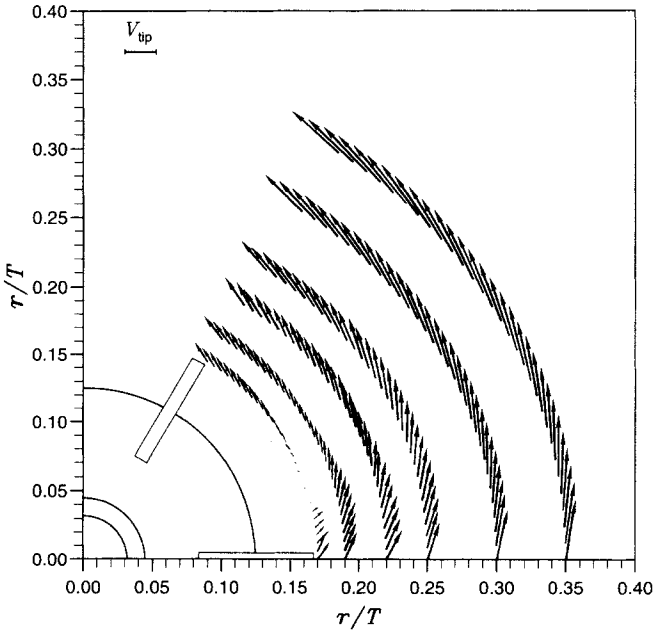

Figure 2. Velocity vectors in the $z/T = 0.35$ plane.

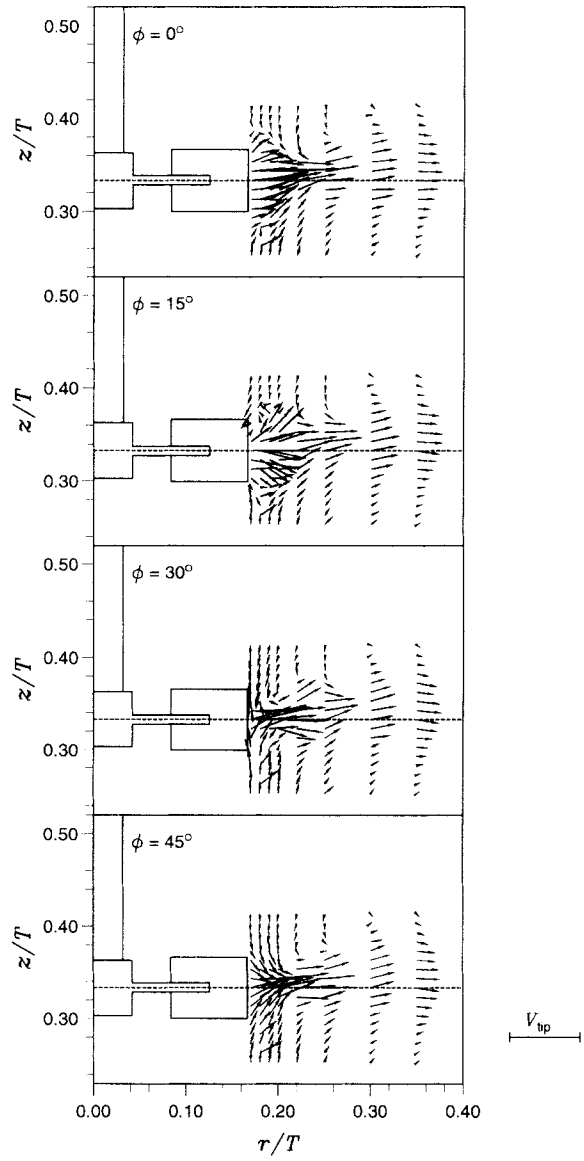

Figure 3. Velocity vectors in the $\phi = 0°$, 15°, 30°, and 45° planes.

and is discussed further below. The flow at radii greater than $r/T = 0.25$ is predominantly tangential, but it is still influenced by the blades.

Figure 3 shows the velocity vectors in four ϕ planes (0°, 15°, 30°, and 45°). A dashed horizontal line is drawn at $z/T = 0.33$ in all ϕ planes in order to aid the assessment of the inclination of the impeller stream. In all ϕ angles, the flows discharged by the impeller are directed towards the vessel wall with a slight upward inclination, on average around 3°–4° to the horizontal. This is in agreement with the previously reported observation of Yianneskis and Whitelaw (1993). The vectors in $\phi = 0°$ and 15° indicate that near the blade (at $r/T = 0.17$ up to 0.30) the impeller stream is inclined upward. The angle of inclination generally decreases with radial distance from the blade tip. By $r/T = 0.35$, the stream is either horizontal ($\phi = 0°$) or inclined downward.

The velocity vectors indicate also the merging of the ring vortices (one of which is formed above and one below the

disk) in the vicinity of the impeller. The formation of these vortices has been previously documented (see, for example, Yianneskis et al., 1987). It can also be seen from Figure 3 that the velocities near the blade tip vary considerably with ϕ. This is indicative of the complex variation of the mean flow behind the blade. In the $\phi = 15°$ plane small circulatory motions can be observed near the upper and lower edges of the blade tip, which indicate the presence of the trailing vortices generated above and below the impeller disk, respectively. It will be shown later that at this blade angle the vortex axis is located at approximately $r/T = 0.17$. The results of Figures 2 and 3 provide evidence that each trailing vortex is contained within a relatively small region. For example, the vortex formed above the disk at $\phi = 15°$ is located between $z/T = 0.34$ and 0.36, approximately.

Trailing vortex axis

The location of the mean axis of the trailing vortex produced by the Rushton impeller is plotted in Figure 4. For comparative purposes the trailing vortex axes determined previously by Van't Riet and Smith (1975), Yianneskis et al. (1987), and Stoots and Calabrese (1995) are also shown.

Van't Riet and Smith utilized a photographic technique to find the shape of the axis by determining the locations where the axial velocity component perpendicular to the axis was zero: as the displacement of the axis in the axial (z) direction is small, the location of the vortex axis can be found by determining the locus where one velocity component perpendicular to the axis is zero. In Yianneskis et al. (1987) and Stoots and Calabrese (1995), as well as in the present work, the vortex axis was determined from angle-resolved LDA mean velocity data, again from the locations where the mean axial velocity component was zero. The discrepancies between the vortex axes presented in these three investigations are attributed to differences between various system characteristics such as the impeller geometry, the clearance of the impeller from the base of the vessel, and the impeller rotational speed.

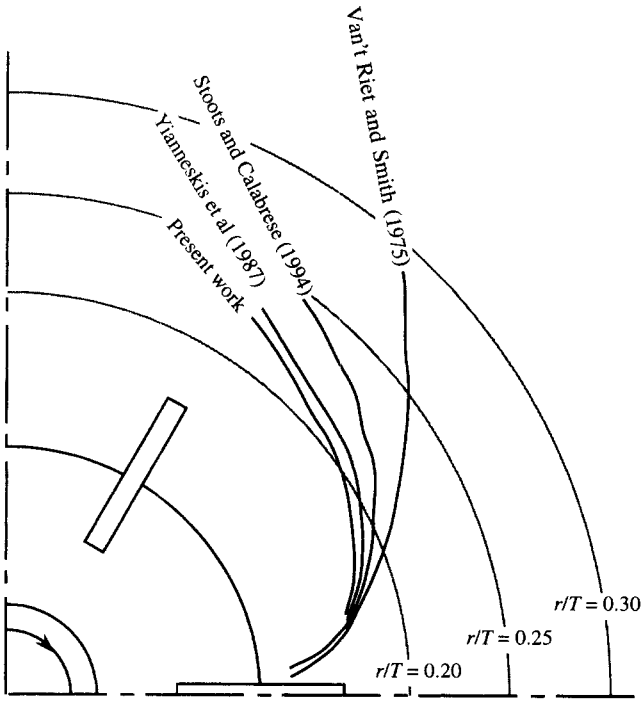

Figure 4. Comparison of the loci of the axis of the trailing vortex.

It can be seen from Figure 4 that the axis of the trailing vortex obtained from the present results is very similar to that reported by Yianneskis et al. (1987). The close agreement of the two axes can be attributed to the geometrical similarities of the vessels and impellers used by Yianneskis et al. and in the present work ($t_b/D = 0.03$ and $C = T/3$). As neither Van't Riet and Smith nor Stoots and Calabrese quote t_b/D values for their impellers and the latter used a clearance $C = T/2$, the observed variation of the present axis from those studies may be due to such geometrical differences, which are known to affect the velocities in the impeller stream (see, for example, Rutherford et al., 1996b).

Velocity variation in the impeller stream

Van der Molen and van Maanen (1978) used vessels from 0.12 m to 0.9 m in diameter with Rushton turbines and found that for fully-turbulent flow, the mean radial velocity just off the tip of the blade and on its center line was a constant ratio (0.85) of the impeller tip speed V_{tip}, and decayed as it moved out along the radius such that

$$\frac{\bar{V}}{V_{tip}} = 0.85\left(\frac{r}{R}\right)^{-7/6} \tag{3}$$

where r is the radial distance (m) and R is the radius of the impeller (m).

For comparison with earlier works, 360° ensemble-averaged mean velocities and turbulence levels were obtained in the impeller disk plane (that is, $z/T = 0.33$); normalized values plotted against r/R are shown in Figures 5a and 5b, respectively. In Figure 5a, the best fits of the data obtained in the present work, by Van der Molen and Van Maanen (1978), and by Dyster et al. (1993), are shown. The best fit of the present data is given by:

$$\frac{\bar{V}}{V_{tip}} = 0.74\left(\frac{r}{R}\right)^{-0.99} \tag{4}$$

The correlation in Eq. 4 agrees very well with that reported by Dyster et al. (1993), but not as well with that obtained by Van der Molen and Van Maanen. Dyster et al. attributed the discrepancies between the best fit of their data and that obtained by Van der Molen and Van Maanen to the minor differences in the impeller geometries and to the fact that the latter used closed-top vessels. However, Nouri and Whitelaw (1990) concluded that the use of a lid affects the flow only in the immediate vicinity of the lid/free surface. Furthermore, the present work was carried out in a vessel with a lid but the data match well those of Dyster et al. Therefore, the discrepancies stem from differences between the impeller geometries employed by Van der Molen and Van Maanen, and by Dyster et al. and the present work.

The best fit of the v'/V_{tip} data obtained in the present work is shown in Figure 5b. The best fit of the present data is given by

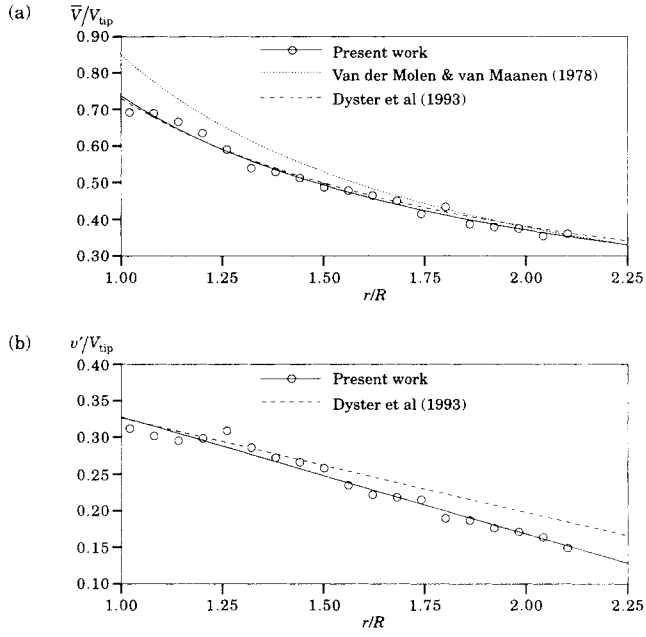

Figure 5. Variation of (a) 360° ensemble-averaged mean velocities and (b) 360° ensemble-averaged RMS velocities with r/R in the $z/T = 0.33$ plane.

$$\frac{v'}{V_{tip}} = 0.48 - 0.16\left(\frac{r}{R}\right) \tag{5}$$

The correlation proposed by Dyster et al. (1993) is:

$$\frac{v'}{V_{tip}} = 0.45 - 0.13\left(\frac{r}{R}\right) \tag{6}$$

is also shown in the figure. The results of the present work show agreement with the data of Dyster et al. near the impeller blade, but the two sets of results diverge with increasing r/R. The reason for this divergence is not clear; however, the local v' values are relatively small (around 0.15 V_{tip}) and it should be noted that there is scatter in both the present data as well as in those of Dyster et al.

Turbulence kinetic energy distributions

Figure 6 shows the turbulence kinetic energy contours in four ϕ planes (0°, 15°, 30°, and 45°). At $\phi = 0°$, the locally high k/V_{tip}^2 levels indicate the presence of the trailing vortices produced by the preceding blade. This region is centered slightly above the impeller disk at $r/T \cong 0.23$ and $z/T \cong 0.34$.

The presence of the trailing vortices produced by the previous blade is still evident at $\phi = 15°$, indicated by a region of k/V_{tip}^2 levels between 0.08–0.10 centered at $z/T = 0.34$, and $r/T = 0.25$. However, k/V_{tip}^2 levels associated with this pair of vortices cannot be distinguished at $\phi = 30°$ and 45°. It is however expected that the elongated shapes of the 0.02–0.08 contours are indeed associated with this pair.

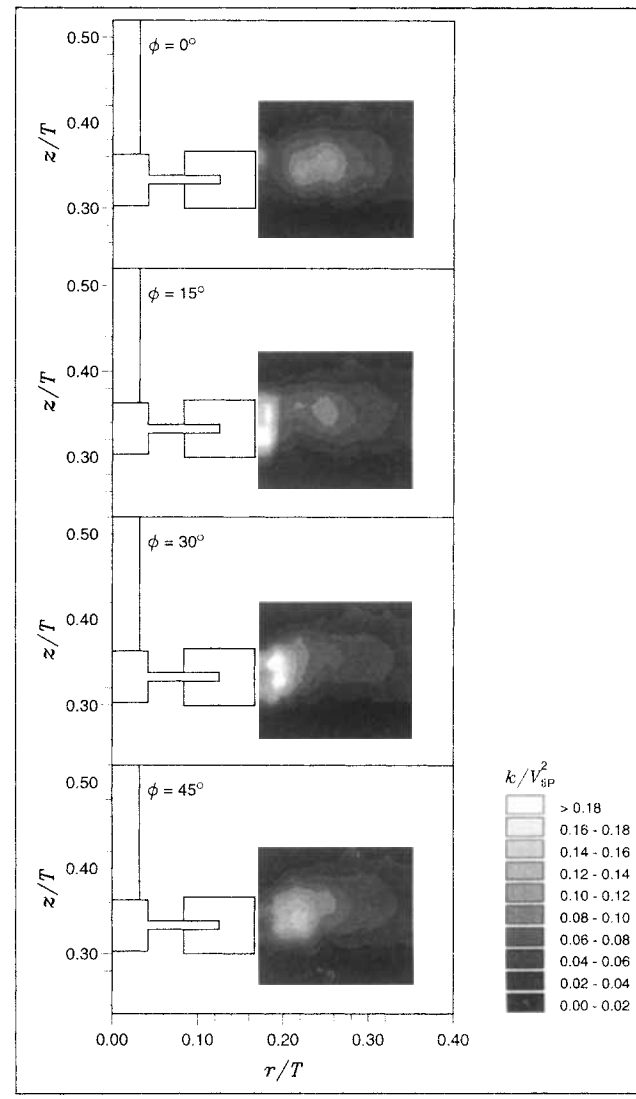

Figure 6. Turbulence kinetic energy contours in the ϕ = 0°, 15°, 30°, and 45° planes.

At $\phi = 15°$, the k/V_{tip}^2 levels above 0.10 near the blade, and the similar k/V_{tip}^2 levels at $\phi = 30°$, and 45°, are associated with the vortex pair generated by the leading blade. The center of this region of high k/V_{tip}^2 is found further out in the impeller stream as ϕ increases, moving from $r/T = 0.17$ at $\phi = 0°$, to $r/T = 0.19$ at $\phi = 30°$, and to $r/T = 0.21$ at $\phi = 45°$.

At all ϕ angles in Figure 6, k/V_{tip}^2 levels above 0.02 are confined to a region which in general is between $z/T = 0.29$ and $z/T = 0.40$. The k/V_{tip}^2 levels become low (< 0.02) and nearly uniform at around 1.5 blade heights above and below the impeller disk.

Figure 7 shows the k/V_{tip}^2 contours in the $z/T = 0.33$ plane. The trailing vortex produced by the leading blade is clearly indicated in this figure and the presence of the trailing vortex generated by the previous blade is also evident.

Isotropy of the impeller discharge flow

In order to ascertain whether the turbulence in the impeller region is isotropic, the distributions of the three turbu-

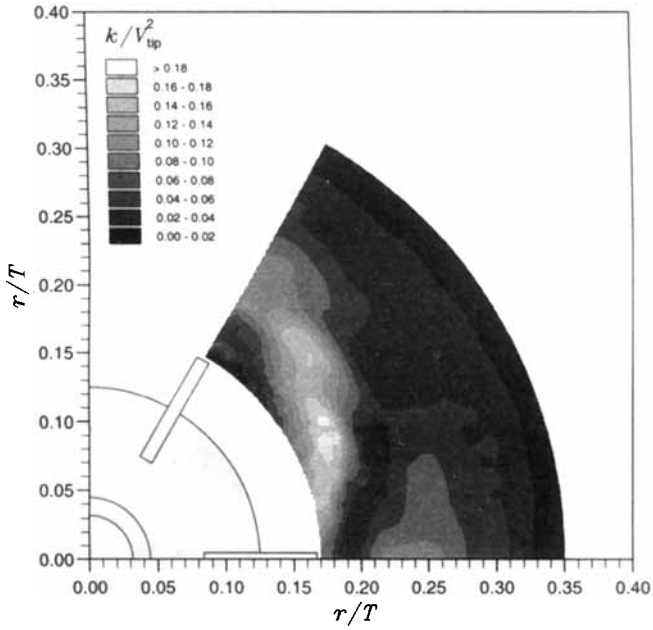

Figure 7. Turbulence kinetic energy contours in the $z/T = 0.33$ plane.

lence levels throughout the measurement region were compared. As the discharge flow out of a Rushton impeller is primarily radial, the turbulence levels of the axial and tangential components were compared with the radial component to quantify the degree of isotropy/anisotropy of the turbulence in the vicinity of the impeller. However, it should be noted that although both the u'/v' and w'/v' values vary from 0.30 to 1.7 in the impeller stream, there are large values of u'/v' and especially w'/v' in the boundaries of the measurement region, where the turbulence levels are quite similar. This is due to the relative magnitudes of the turbulence levels, for example, for $w' = 0.02$ and $v' = 0.01$, $w'/v' = 2.0$, whereas in absolute terms the levels are similar and within experimental error. A better way to assess the degree of isotropy is by considering the absolute difference between the different turbulence levels normalized by V_{tip}, that is, $|u' - v'|/V_{tip}$ and $|w' - v'|/V_{tip}$. When these values tend to zero, $u' \to v'$ and $w' \to v'$ and the turbulence may be considered isotropic.

Contours of $|u' - v'|/V_{tip}$ in the $\phi = 0°$, 15°, 30° and 45° planes are shown in Figure 8. Regions of locally high values of $|u' - v'|/V_{tip}$ can be observed near the impeller blade in all ϕ planes. Most of the regions near the edges of the measurement area have values of $|u' - v'|/V_{tip}$ between 0.00 and 0.02. In these regions, the turbulence may be considered to be isotropic. Locally high values of $|w' - v'|/V_{tip}$ were also observed near the blade in all ϕ planes.

The results presented in this section indicate that the turbulence in the impeller stream deviates from isotropy. Further away from the impeller, the deviation becomes smaller and the turbulence might be regarded as isotropic.

Time-resolved velocities and normalized energy spectra

In order to quantify the decay of the trailing vortex structure away from the blades, time-resolved velocity measure-

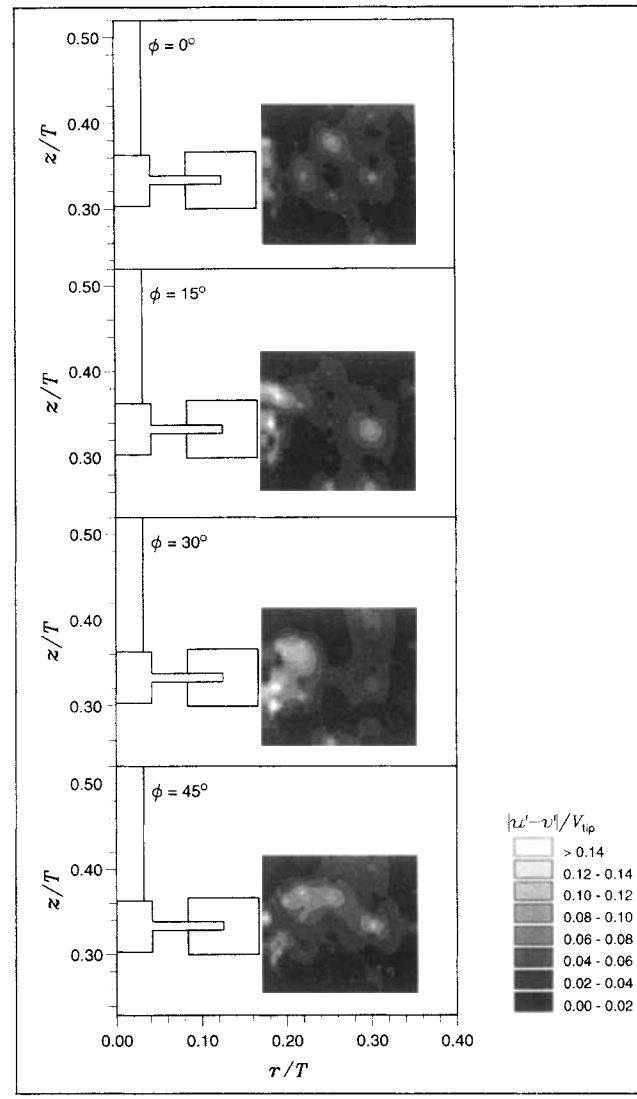

Figure 8. $|u' - v'|/V_{tip}$ contours in the $\phi = 0°$, 15°, 30°, and 45° planes.

ments of the radial component were made in the impeller stream at the $z/T = 0.33$ plane. Both Stoots and Calabrese (1995) and Yianneskis and Whitelaw (1993) showed that a cyclic variation of the velocity is obtained with each blade passage in the vicinity of the trailing vortices. The expected six cycles (blade crossings) per revolution were clearly defined in the instantaneous radial velocity recordings obtained at $r/T = 0.17$ and $r/T = 0.18$, while further away from the impeller, at $r/T = 0.22$, although cyclic fluctuations were still discernible, their magnitude had decreased, while at $r/T = 0.25$, fluctuations of the velocity behind some, but not all, blades were discernible.

A better way to assess the influence of periodicity to the flow is by quantifying the changes of the strength of the frequency components along the impeller stream, therefore, spectral analysis of the velocity recordings was performed. Since velocity realizations with LDA are obtained at random intervals, the Lomb method, which is a method of spectral analysis for unevenly sampled data, was employed to obtain the normalized energy spectrum, $P(f) = E'(f)/u'^2$ in the

manner described by Press et al. (1992). The energy spectrum $E(f)$ (m^2/s) was calculated using pseudo-equi-time spaced data in the manner described in the following section. $P(f)$ spectra are useful to identify discrete frequencies in the flow. They are not presented here to avoid partial duplication with the $E(f)$ spectra which are presented below.

The normalized energy spectra of the velocity recordings at $r/T = 0.17$, $r/T = 0.18$, and $r/T = 0.22$ at $z/T = 0.33$ exhibited a peak at the spectral frequency of 216 Hz, indicating a well-defined periodic motion, which corresponded to the blade passage frequency. The magnitude of this peak at $r/T = 0.22$ decayed to about 20% of that found at $r/T = 0.17$, indicating that the periodic motion in the flow at this location is not as pronounced, while in the normalized spectrum of the velocity recording made at $r/T = 0.25$ no distinctive peak could be observed, indicating that the vortex structure has begun to break down into random turbulence. This trend is in agreement with Mujumdar et al. (1970), who observed that 80% to 90% of the turbulence intensities measured close to the impeller blade were due to the periodic component and that this component decayed quickly to a negligible value at about 0.66 of the tank radius (that is, $r/T = 0.33$).

Energy spectra and scales of turbulence

It is useful to compute the energy spectrum $E(f)$ to describe a turbulent flow, especially to quantify the slope of the spectrum at high frequencies. The instantaneous velocity U (m/s) can be expressed as

$$U = \overline{U} + u \tag{7}$$

where U is the instantaneous velocity, $\overline{U}$ is the average value of U and u is the fluctuating velocity component. The one-dimensional energy spectrum $E(f)$ is obtained from the Fourier transform of u^2 and represents the energy contained between frequencies (Hz) f and $f + df$ such that:

$$u'^2 = \int_0^\infty E(f)\, df \tag{8}$$

and

$$u' = \sqrt{\overline{u}^2} \tag{9}$$

The velocity realizations with LDA are obtained at random intervals and therefore complications are introduced in the calculation of $E(f)$. However, it is possible to obtain pseudo-equi-time spaced data by conditionally resampling the velocity recording (see, for example, Durao et al., 1980). In order to determine a suitable resampling interval, each velocity recording was resampled with various resampling intervals. The resampling interval of each recording was then selected by comparing the normalized energy spectra obtained from the resampled records with those obtained from the raw data such that the resampling process did not distort the raw data.

In order to obtain the $E(f)$ of the real turbulence, it is necessary to correct the velocity fluctuations to account for the periodic component present in the flow (that is, the pseudo-turbulence). A number of methods can be employed to obtain the real turbulence velocity component, for example, by subtracting the 1° ensemble-averaged mean velocities from the instantaneous velocities, or by estimating the instantaneous mean velocities using the moving-window averaging method. However, the former method generally does not yield a zero-mean velocity fluctuation due to cycle-to-cycle variations (see, for example, Yianneskis and Whitelaw, 1993), while the latter acts as a high-pass filter and thus information on low-frequency turbulence will be lost. Therefore, a band-stop frequency filtering technique was employed in the present work.

Figure 9 shows the energy spectra of the corrected radial velocity recordings obtained at $r/T = 0.17$, 0.19 and 0.21, plotted in log-log scales. A straight line of $-5/3$ slope is also drawn on the figure, which represents the energy distribution predicted by Kolmogorov from a dimensional analysis for the inertial subrange (Nishikawa et al., 1976; Landahl and Mollo-Christensen, 1986). Although the $-5/3$ slope in the spectrum does not prove the existence of local isotropy, it has been employed to lend confidence to the approximation of local isotropy (Kresta and Wood, 1993). Few or no regions with a $-5/3$ slope can be observed in the energy spectra at $r/T = 0.17$ and 0.19. The difference between the slope of the spectrum obtained at $r/T = 0.21$ and the $-5/3$ line is also large at low frequencies, however, a small region with a $-5/3$ slope at frequencies above approximately 2 kHz can be observed.

Figure 10 shows the energy spectra further away from the impeller at $r/T = 0.31$, 0.33 and 0.35. Regions with $-5/3$ slope can be observed for all three energy spectra for frequencies above about 200 Hz.

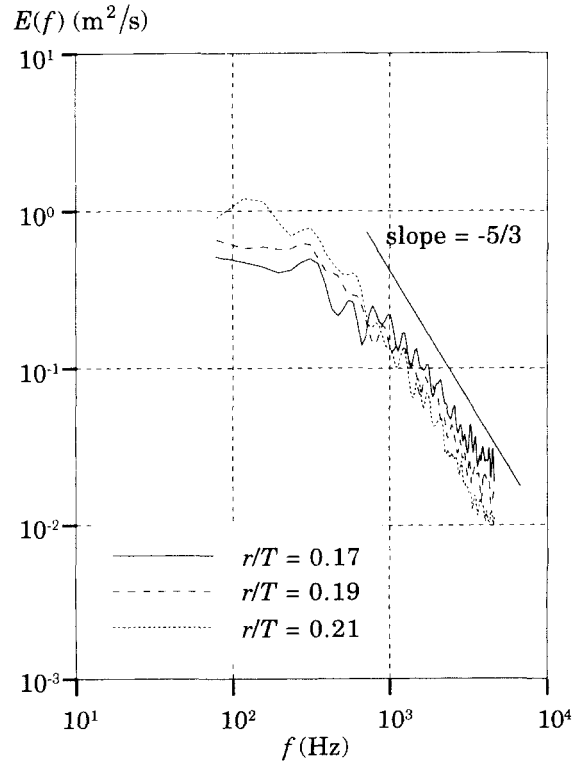

Figure 9. Energy spectrum of the radial velocity (with the periodic component removed) at $r/T = 0.17$, 0.19 and 0.21, $z/T = 0.33$.

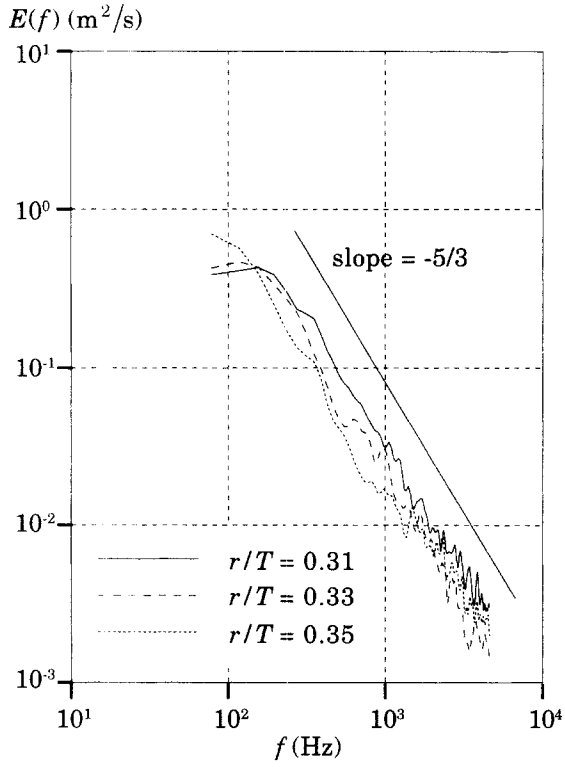

Figure 10. Energy spectrum of the radial velocity (with the periodic component removed) at $r/T = 0.31$, 0.33 and 0.35, $z/T = 0.33$.

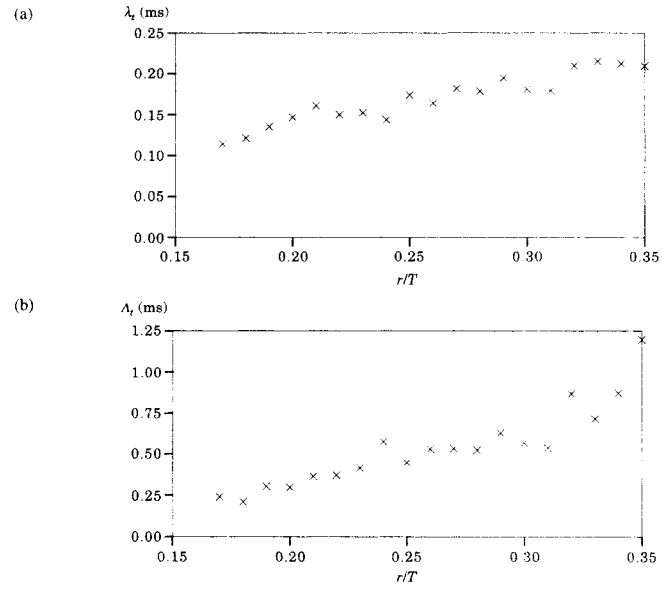

Figure 11. Variation of (a) microtime scales; and (b) integral time scales with r/T at $z/T = 0.33$ in the $\theta = 0°$ plane.

Temporal scales of turbulence

A characterization of the eddy-size distribution within a turbulent flow can be obtained from the autocorrelation of the velocity fluctuations. The autocorrelation function coefficient is defined by Eq. 10, and can be obtained by the Fourier transform of $E(f)/u'^2$

$$R(\tau) = \frac{\overline{u(t)u(t+\tau)}}{u'^2} \tag{10}$$

where t is time and τ is the correlation time(s). The integral time scale of turbulence Λ_t (ms) is defined as:

$$\Lambda_t = \int_0^\infty R(\tau)\, d\tau \tag{11}$$

Although the integral time scale is defined as the integral of $R(\tau)$ from zero to infinity, in practice it is computed to the first zero of the autocorrelation function (Yianneskis et al., 1991). The micro time scale $\lambda_{t(\text{ms})}$ is given by:

$$\frac{-2}{\lambda_t^2} = \left(\frac{\partial^2 R(\tau)}{\partial t^2}\right)_{t=0} \tag{12}$$

The autocorrelation function coefficients $R(\tau)$ of the corrected instantaneous radial velocity variation at various r/T locations were computed from the energy spectra using an FFT technique. From the $R(\tau)$ obtained, Λ_t and λ_t were computed using Eqs. 11 and 12, respectively. The variations of the micro and integral time scales with r/T at $\theta = 0°$, and $z/T = 0.33$, are shown in Figures 11a and 11b, respectively.

The distribution of micro time scales in Figure 11a shows that λ_t is about 0.11 ms at $r/T = 0.17$, and increases gradually to around 0.20 ms at $r/T = 0.35$. In Figure 11b, it can be seen that Λ_t is small (0.25 ms) near the impeller blade at $r/T = 0.17$ and increases gradually to approximately 0.35 ms at $r/T = 0.25$ and to around 1.24 ms at $r/T = 0.35$. This distribution might be expected since the velocities near the impeller are higher and the corresponding time scales are therefore shorter. The integral time scales are approximately 3–6 times higher than the corresponding micro time scales.

Spatial scales of turbulence

Spatial scales of turbulence can be obtained by multiplying the temporal scales with an appropriate convective velocity. G. I. Taylor (see Lancaster, 1976) showed that temporal and spatial scales of turbulence could be related by:

$$\Lambda_x = \Lambda_t \overline{U} \tag{13}$$

and

$$\lambda_x = \lambda_t \overline{U} \tag{14}$$

where Λ_x and λ_x (mm) are the integral and micro length scales respectively. However, Eqs. 13 and 14 are accurate only when $\overline{U}$ constant and the relative turbulence intensity is much smaller than unity (that is, $\overline{U} \gg u'$), which is true for flows at low Reynolds number when the turbulence of the flow moving past a location is effectively frozen (Hinze, 1975). Both conditions are not satisfied in many parts of the flow studied here, since the Reynolds number is large and the mean flow in the vicinity of the impeller stream is periodic.

An alternative convective velocity has been suggested for high Reynolds number flows by Heskestad (1965), to better account for the coupling of micro time and length scales in a nonswirling flow, that is, where the tangential mean velocity is zero. However, this is not true in the present work where a strong tangential flow is induced by the impeller and it is inappropriate to apply Heskestad's suggestion. Therefore, Λ_x and λ_x were estimated using Eqs. 13 and 14 respectively, with the local ensemble-averaged mean velocities as the convective velocities. The scales computed are shown only as approximate indications of eddy sizes, as the conditions mentioned above are not satisfied in all locations concerned.

The distribution of Λ_x along the impeller stream at $z/T = 0.33$ in the $\theta = 0°$ plane is shown in Figure 12. It can be observed that Λ_x has a minimum value of around 0.6 mm at $r/T = 0.17$, approximately equal to 0.1 W, and increases with increasing r/T, reaching a maximum value of about 1.7 mm at $r/T = 0.35$, approximately equal to 0.3 W. The values of Λ_x obtained in the present work are somewhat smaller than those reported previously. Cutter (1966), who conducted experiments in a $T = 292$ mm vessel, obtained values of Λ_x of approximately 0.2 W and 0.4 W at $r/T = 0.17$ and 0.35 respectively; Mahouast et al. (1989) reported a minimum value of approximately 0.48 W and a maximum of around 1.32 W for Λ_x in the impeller stream in a $T = 200$ mm vessel; and minimum and maximum values of 0.1 W and 0.4 W for Λ_x were reported by Wu and Patterson (1989). Notwithstanding the different methods employed to calculate Λ_x by the various researchers, there is good agreement between the values measured in this work and those reported by Cutter and by Wu and Patterson. Mahouast et al.'s Λ_x values are higher and do not agree well with either the present findings or those of Cutter and Wu and Patterson. The above comparisons of the reported integral length scale values indicate that the frequently employed assumption that $\Lambda_x = 0.1\ D$ (that is, around 0.4 W in this work) near the blade tip (Kresta, 1991) is not considered to be appropriate as it provides an overestimation of Λ_x.

The values of λ_x are not presented as they remained almost constant with increasing r/T; the average value of λ_x was around 0.25 mm (0.03 W). This value compares well with those reported by Wu and Patterson, who obtained micro length scales of 0.02 to 0.07 W in the impeller stream. However, λ_x might be expected to increase with r/T; and the near-constant variation obtained is likely to stem from the approximations and corresponding uncertainties involved in its determination.

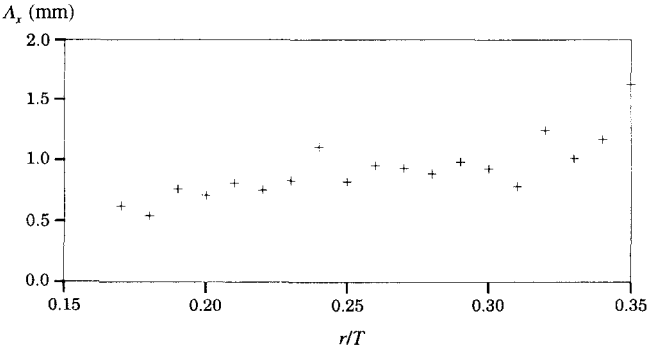

Figure 12. Variation of integral length scales with r/T at $z/T = 0.33$ in the $\theta = 0°$ plane.

Dissipation rate of kinetic energy of turbulence

The rate of dissipation of turbulence kinetic energy ϵ is a parameter of great interest both for the characterization of turbulence and the identification of regions where energy is dissipated in stirred vessels. Furthermore, as most CFD prediction methods employ the k-ϵ turbulence model, knowledge of the local energy dissipation rate is very important. Several methods have been proposed for the determination of ϵ. Wu and Patterson (1989) proposed that

$$\epsilon = \frac{0.85k^{3/2}}{\Lambda_f} \tag{15}$$

The values of ϵ in the $\theta = 0°$ plane were calculated in the present work using both Eq. 15 with $\Lambda_f = (3\Lambda_x^2)^{1/2}$ and $\epsilon = \overline{(u^2)}^{3/2}/\Lambda_x$. In order to allow comparisons with the estimates of Patterson and Wu (1985), the values of k were obtained from the 60° ensemble-averaged turbulence levels, while the values of Λ_x presented above were used. The variation of ϵ, normalized with N^3D^2, with (r/R) at $z/T = 0.33$ is shown in Figure 13. For comparison purposes, the results reported by Patterson and Wu are also shown in the figure. It can be observed that the value of ϵ/N^3D^2 decreases from around 22 near the blade tip to values comparable with those of Patterson and Wu at $r/R = 1.5$. The values obtained in the present work are generally higher than those reported by Patterson and Wu. It should be noted that Patterson and Wu found that near the blade tip ϵ/N^3D^2 increases with rotational speed, but further away it is not strongly affected. Therefore, the relatively high ϵ/N^3D^2 values at $r/R < 1.5$ in the present work may be attributed to the higher speed (2,165 rpm compared with 200 rpm in Patterson and Wu) employed here. This might have important implications for the scaling of stirred reactor flows and should be investigated further. In addition, ϵ values calculated using the angle-resolved values of k in the impeller stream compare well with the corresponding results of Stoots and Calabrese (1996).

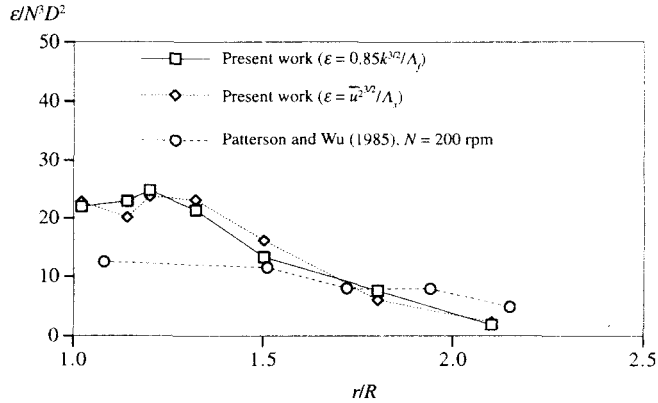

Figure 13. Variation of the normalized rate of dissipation of k with r/R at $z/T = 0.33$ in the $\theta = 0°$ plane.

Furthermore, it can be seen from Eq. 15 that ϵ is a function of k and Λ_x or Λ_f; therefore, the accuracy of ϵ depends on the accuracy of Λ_x. However, as mentioned earlier, the calculation of Λ_x using Eq. 13 is only accurate when $\bar{U}$ is constant and $\bar{U} \gg u'$, which is not true in the flow studied. This may therefore introduce inaccuracies in the ϵ values obtained.

Finally, the anisotropy of the impeller stream turbulence shown in this work should be taken into consideration in CFD predictions of the flows, most of which employ the k-ϵ model of turbulence, in the formulation of which there is an assumption of isotropic eddy viscosity. Although the formulation of the model only implicitly implies isotropy of turbulence (Abbot and Basco, 1989), Tatterson (1991) reported that of the predictions which employed the k-ϵ model, those which made use of a three-dimensional nonisotropic version of the model provided the most realistic simulation of the flowfield. Similarly, comparisons of CFD predictions of the flow (El-Wazzan, 1997) using the k-ϵ model and a Reynolds-stress model with experimental data have shown that the latter model yielded k values which are closer to the measurements. Bakker (1992) has observed that the k-ϵ model underpredicted turbulence levels in the impeller stream, where the flow has been shown to be anisotropic in the present study. In addition, the shortcomings of the k-ϵ model in three-dimensional flows with strong streamline curvature are well known. Similarly, the presence of a region with a $-5/3$ slope in the spectra has been employed to support the assumption of local isotropy (see, for example, Kresta and Wood, 1993). The deviation of the slopes of the spectra from the value of $-5/3$ near the blade and the progressive tendency of the spectra toward a $-5/3$ slope with increasing distance from the blade should also be taken into consideration in the future when the impeller stream turbulence is characterized.

Concluding Remarks

LDA results obtained in a 100 mm diameter vessel have been presented, and the flowfield and turbulence structure produced in the vicinity of a Rushton impeller has been described in detail. The location of the trailing vortex axis was also determined and compared with the results of earlier investigations. The degree of anisotropy of the turbulence in the vicinity of the impeller blades decreases with distance from the blade tip, as indicated by comparison of the three normal stress components.

Micro and integral time scales calculated from time-resolved measurements had values of 0.11–0.2 ms and 0.22–1.24 ms, respectively. The periodicity of the flow was established through spectral analysis, and estimates of length scales and ϵ were provided. The integral length scales estimated exhibited minimum and maximum values in the impeller stream of 0.1 and 0.3 W, respectively, which are in general agreement with previously reported data. The frequently employed assumption that the macro length scale is around 0.1 D may provide an overestimation of the length scale by a factor of 2 near the blade tip.

The turbulence scale and kinetic energy dissipation data presented above are in agreement with a number of previously reported studies, but the differences between the results of the various investigations indicate clearly that better defined techniques for the characterization of such quantities are necessary. Clearly, the application of two-point anemometry would enable spatial correlations to be obtained and thus it might be possible to determine more accurate length scales and ϵ values. As the accurate determination of ϵ is crucial for a better understanding and prediction of mixing processes, such work is urgently needed.

Notation

h = impeller blade height, m
k = turbulence kinetic energy, m^2/s^2
Re = Reynolds number
$R(\tau)$ = autocorrelation function coefficient
V = instantaneous radial velocity, m/s
V_r = rotational speed ($= 2\pi Nr$), m/s
z = axial co-ordinate of the measurement volume, m
ϵ = rate of dissipation of kinetic energy of turbulence, m^2/s^3

Literature Cited

Abbott M. B., and D. R. Basco, *Computational Fluid Dynamics: An Introduction for Engineers*, Wiley, New York (1989).

Bakker A., "Hydrodynamics of Stirred Gas-Liquid Dispersions," PhD Thesis, Delft Univ. of Technology, The Netherlands (1992).

Cutter, L. A., "Flow and Turbulence in a Stirred Tank," *AIChE J.*, **12**(1), 35 (1966).

Durao, D. F. G., J. Laker, and J. H. Whitelaw, "Bias Effects in Laser Doppler Anemometry," *J Phys. E: Sci. Instrum.*, **13**, 442 (1980).

Dyster, K. N., E. Koutsakos, Z. Jaworski, and A. W. Nienow, "An LDA Study of the Radial Discharge Velocities Generated by a Rushton Turbine: Newtonian Fluids, $Re \geq 5$," *Trans IChemE*, **71**, Part A, 11 (1993).

El-Wazzan, Y. J. E., "The Prediction of Swirling Recirculating Flow and the Fluid Flow and Mixing in a Stirred Tank," PhD Thesis, Univ. of London (1997).

Heskestad, G., "A Generalized Taylor's Hypothesis with Application for High Reynolds Number Turbulent Shear Flows," *Trans. ASME J. Applied Mech.*, **32**, 735 (1965).

Hinze, J. O., *Turbulence*, McGraw Hill, London (1975).

Kresta, S. M., "Characterization, Measurement and Prediction of the Turbulent Flow in Stirred Tanks," PhD Thesis, McMaster Univ., Canada (1991).

Kresta, S. M., and P. E. Wood, "The Flow Field Produced by a Pitched Blade Turbine: Characterisation of the Turbulence and Estimation of the Dissipation Rate," *Chem. Eng. Sci.*, **48**(10), 1761 (1993).

Lancaster, D R., "Effects of Engine Variables on Turbulence in a Spark-Ignition Engine," SAE paper No. 760159 (1976).

Landahl, M. T., and E. Mollo-Christensen, *Turbulence and Random Processes in Fluid Mechanics*, Cambridge University Press, Cambridge, U.K. (1986).

Mahouast, M., G. Cognet, and R. David, "Two-Component LDV Measurements in a Stirred Tank," *AIChE J.*, **35**(11), 1770 (1989).

Mujumdar, A. S., B.Huang, D. Wolf, M. E. Weer, and W. S. M. Douglas, "Turbulence Parameters in Stirred Tank," *Can. J. Chem. Eng.*, **48**, 475 (1970).

Nishikawa, M., Y. Okamoto, K. Hasimoto, and S. Nagata, "Turbulence Energy Spectra in Baffled Mixing Vessels," *J. Chem. Eng. Japan*, **9**(6), 493 (1976).

Nouri, J. M., and J. H. Whitelaw, "Effect of Size and Confinement on the Flow Characteristics in Stirred Reactors," paper 23.2, *Proc. Int. Symp. on Application of Laser Techniques to Fluid Mechanics*, Lisbon, Portugal (1990).

Patterson, G .K., and H. Wu, "Distribution of Turbulence Energy Dissipation Rates in Mixers," *Proc Eur. Conf. on Mixing*, BHRA Fluid Engineering, Wurzburg, West Germany (1985).

Press, W. H., B. P. Flannery, S. A. Teukolsky, and W. T Vetterling, *Numerical Recipes, The Art of Scientific Computing*, Cambridge University Press (1992).

Rutherford, K., K. C. Lee, S. M. S. Mahmoudi, and M. Yianneskis, "Hydrodynamic Characteristics of Dual Rushton Impeller Stirred Vessels," *AIChE J.*, **42**(2), 332 (1996a).

Rutherford, K., K.C. Lee, S. M. S. Mahmoudi, and M. Yianneskis,

"The Influence of Rushton Impeller Blade and Disk Thickness on the Mixing Characteristics of Stirred Vessels," *Trans. I.Chem.E.*, **74**, Part A, 369 (1996b).
Stoots, C. M., and R. V. Calabrese, "The Mean Velocity Field Relative to a Rushton Turbine Blade," *AIChE J.*, **41**(1),1 (1995)
Stoots, C. M., and R. V. Calabrese, Personal Communication (1996).
Tatterson G. B., *Fluid Mixing and Gas Dispersion in Agitated Tanks*, McGraw-Hill, New York (1991).
Uhl, V. W., and J. B. Gray, *Mixing, Theory and Practice*, Academic Press, London (1966).
Van Der Molen, K., and H. R. E. van Maanen, "Laser-Doppler Measurements of the Turbulent Flow in Stirred Vessels to Establish Scaling Rules," *Chem. Eng. Sci.*, **33**, 1161 (1978).
Van't Riet, K., and J. M. Smith, "The Trailing Vortex System Produced by Rushton Turbine Agitators," *Chem. Eng. Sci.*, **30**, 1093 (1975).
Van't Riet, K., W. Bruijn, and J. M. Smith, "Real and Pseudo-Turbulence in the Discharge Stream from a Rushton Turbine," *Chem. Eng. Sci.*, **31**, 407 (1976).
Wu, H., and G. K. Patterson, "Laser-Doppler Measurements of Turbulent-Flow Parameters in a Stirred Mixer," *Chem. Eng. Sci.*, **44**(10), 2207 (1989).
Yianneskis, M., and J. H. Whitelaw, "On the Structure of the Trailing Vortices around Rushton Turbine Blades," *Trans. I. Chem. E.*, **17**, Part A, 543 (1993).
Yianneskis, M., Z. Popiolek, and J. H. Whitelaw, "An Experimental Study of the Steady and Unsteady Flow Characteristics of Stirred Reactors," *J. Fluid Mech.*, **175**, 537 (1987).
Yianneskis, M., M. J. Tindal, and S. Nadarajah, "Measurement of Turbulence Scales, Moments and Spectra in Engine Flows," *Proc. I. Mech. E.: Experimental Methods in Engine Research and Development*, 127 (1991).

Manuscript received Mar. 4, 1997, and revision received July 18, 1997.